DSM GENERATION FROM HIGH RESOLUTION SATELLITE IMAGERY USING ADDITIONAL INFORMATION CONTAINED IN EXISTING DSM

D. Hoja*, P. Reinartz, M. Lehner

DLR, Remote Sensing Technology Institute, 82234 Weßling, Germany - (Danielle.Hoja, Peter.Reinartz, Manfred.Lehner)@dlr.de

Commission I, WG I/5

KEY WORDS: DEM Generation, DSM, Optical Stereo Data, InSAR, Triangulation, DSM Integration

ABSTRACT:

Information about the shape of the Earth's surface are required for several tasks like the creation of orthoimages or flood control. The generation of digital elevation models (DEM) with stereo images from space, or with interferometric synthetic aperture radar (InSAR) have been proven to be reliable and cost effective for larger regions, especially in remote areas and developing countries. Instead of a DEM, a digital surface model (DSM) is generated with remote sensing methods. Optical stereo image pairs are matched to get a large number of automatically located conjugate points. These points are mapped by forward intersection into the object space. The DSM is retrieved from these points by triangulation and interpolation. This method is mainly used to generate DSM from scratch. Thereby, the matching of optical images results often in areas without matching points, e.g. due to low contrast. This paper follows the approach to include the information of existing InSAR DSM into the point data set before or during the DSM generation from optical stereo images. Several methods are discussed and a SPOT image pair is analysed. Comparisons are shown for two interpolations with and without additional input. Advantages of using the single data sets and of the combined data sets are discussed.

1. INTRODUCTION

Information about the shape of the Earth's surface are required for several tasks like the creation of maps and perspective views, urban planning, and flood control. Digital elevation models (DEM) are generated by traditional photogrammetry with aerial photos, by airborne laser scanning, with stereo images from space, or with interferometric synthetic aperture radar (InSAR) (Jacobsen, 2004). From these methods, the last two have been proven to be reliable and cost effective for larger regions, especially for the DEM generation of up to now poorly mapped regions.

The manual measurement of DEM is too time consuming, so most of the data processing is done by automatic programs, e.g. optical image matching. Instead of a DEM, a digital surface model (DSM) is generated with remote sensing methods (except laser scanning). The DSM represents the visible surface, including vegetation and buildings. The conversion of a DSM into a DEM is another task of research in remote sensing (Baltsavias, 1999). Tools have been developed to eliminate points not located on the Earth surface resulting in a DEM.

Data sets of different sensors are available for optical DSM generation with high (SPOT-5 HRS, 10 m) and very high resolution (IKONOS, 1 m) for this study. First, these stereo image pairs are matched to get a large number of automatically located conjugate points (Lehner & Gill, 1992). In the second step, the DSM is retrieved from these points by triangulation and interpolation. InSAR uses phase information from two SAR images of the same area for DSM generation. For the world's landmass between ±60°, a complete DSM was generated with data of the Shuttle Radar Topography Mission (SRTM) in 2000 (Eineder et al., 2000).

The described methods are mainly used to generate DSM from scratch, i.e. every time a completely new DSM is generated.

The matching of optical images results often in areas without points, e.g. due to low contrast. Also in InSAR DSM gaps occur due to radar shadow and layover, especially under extreme conditions like in high mountain terrains. Up to now, only DEM fusions after the generation have been carried out (Reinartz et al., 2004). This paper follows the approach to include the information of existing InSAR DSM into the point data set before or during the DSM generation from optical stereo images. Two methods are discussed.

Different optical data sets from SPOT and IKONOS are analysed. Test site is an area in southern Bavaria, containing a wide range of heights. As existing InSAR DSM, different InSAR DSM are used. The interpolation is carried out for the original data set from optical stereo data with and without integration of additional points from the InSAR DSM. Comparisons are shown for the two interpolations. Advantages of the different data sets are discussed.

2. ESTABLISHED DEM GENERATION METHODS

2.1 Matching of Stereo Image Pairs

The derivation of digital elevation models from optical stereo image data consists of two main tasks. During image matching a large number of conjugate points is extracted from the stereoscopic imagery. The algorithm used is based on areal matching in image pyramids and subsequent local least squares matching. These conjugate points are then converted with photogrammetric adjustment software based on collinearity equations into 3D points in the final projection. A detailed description of the whole process can be found in (Lehner & Gill, 1992). Here, only a short description of the main steps is given.

---

* Corresponding author.

In images with high and very high resolutions, large homogeneous areas like fields, meadows, and water bodies appear where good patterns for image correlation cannot be extracted. For automatic image matching, an interest operator automatically selects patterns which are well suited for digital image correlation. The interest operator used is based on the so-called "Förstner operator" (Förstner & Gülch, 1987).

For area based matching, corresponding search areas have to be extracted from the scene of the second looking direction. This is accomplished by computing a local affine transformation between the stereo partners. The transformation parameters are calculated by least squares adjustment using already known conjugate points. At the lowest resolution level of the image pyramid, a few manually defined conjugate points are used to start the process.

A matrix of normalized correlation coefficients is computed for the given pattern found by the interest operator and the search areas in the second scene. The given pattern is shifted pixel by pixel over the search area. The maximum of the correlation coefficients defines the location in the search area corresponding to the centre pixel of the pattern area with pixel accuracy. This correlation has to meet two acceptance rules: the maximum of the correlation coefficient being beyond a given threshold and the point not lying on the border of the correlation coefficient matrix. Finally, local least squares matching techniques as described in (Ackermann, 1984) are used to refine the results to subpixel level.

The quality of the matching is controlled by forward and backward matching of the two stereo partners using the local least squares matching method. The dense image matching, which uses nearly every pixel as a kernel centre for Otto-Chau region growing (Heipke et al., 1996), provides parallaxes for most pixels. For the found pairs of conjugate points, the ground coordinates including their heights (3D points) are calculated by forward intersection using the interior and exterior orientation of the camera during imaging.

The automatic image matching depends on corresponding, but not necessary identical grey patterns in the conjugate image areas (Jacobsen, 2004). Areas with steep slopes, shadows, forests, snow and ice fields are likely to have problems in the correlation process. Errors caused by such failure of correlation normally introduce spikes into the resulting DEM (Guoan, 2000). To prevent such errors, all points (i.e. the matched areas around the points) are checked by strict acceptance rules as described above. Only points passing this test are used for the following interpolation. However, areas of low contrast in the images result in a lower point density. Large areas can occur with no conjugate points resulting in a digital height model with low accuracy at such places. The method described in chapter 3 shows a way to overcome this problem.

2.2 Triangulation and Interpolation

Result of matching and forward intersection is a set of 3D points representing the Earth surface (including i.e. tree tops) acquired by the stereo images. To ease further applications, the irregular point cloud has to be transferred to a regularly spaced grid model. This regularization is carried out in two steps. First, the points are connected by Delauney triangulation into a triangulated irregular network (TIN). These triangles are then used for interpolation of a regularly spaced grid.

A triangulation divides a surface into triangles connecting all given points to the triangle network. The Delauney triangulation is a special triangulation for a set of points such that no point is inside the circumcircle of any other triangle. This triangulation has some desirable features. The triangles are

as equilateral as possible. Thin wedge shaped triangles are avoided. The triangulation is unique for all but trivial cases (e.g. four points describing a rectangle).

The triangulation method used is based on the 'algorithm for interpolating irregularly-spaced data with application in terrain modeling' (Bourke, 1989). It is specially developed to handle a large number of points independent of different point densities in various regions of the point cloud. A special feature of this algorithm is the possibility to add further points obtained later to the existing triangulation without executing a completely new triangulation. However, due to the large memory and fast processors of current computers, this is only valid to integrate single points. Adding of a large number of points is faster by carrying out a completely new triangulation by the current implementation of the algorithm. This avoids the time consuming step to check all triangles for each new point if it is inside.

Finally, the triangles are superimposed on the regularly spaced grid of the resulting DEM. For each triangle the plane defined by the three vertices is calculated. To each pixel inside the triangle the height value interpolated on this plane is assigned.

Figure 1 shows the result of the described algorithm for the test area in southern Bavaria. A detailed description of the test site can be found in chapter 4. The SPOT stereo image pair was acquired on October 1, 2002 by along-track stereoscopy. The automatic image matching results in 7719964 conjugate points. Up to nine of these points are inside one pixel (25 m × 25 m); therefore only 3030500 points are used in the triangulation. 6060914 triangles are input to the interpolation.
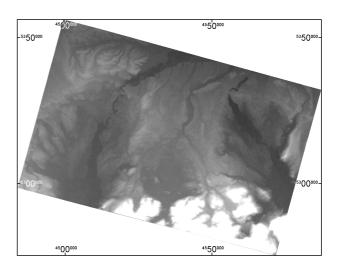

Figure 1. DSM resulting from matching of a SPOT stereo image pair acquired on October 1, 2002 and following triangulation of 7.7 Mio. object space points.

2.3 Interferometric SAR

The analysis of two synthetic aperture radar (SAR) images of the same area acquired under slightly different incidence angles is called interferometric SAR (InSAR). Points with the same distance to a single antenna cannot be distinguished in a SAR image. The usage of a second antenna position dissolves this ambiguity and can therefore be used for height model generation. InSAR uses the phase information contained in complex SAR data and the direct proportionality of the phase difference to object height variations.

InSAR processing includes a number of single steps. A detailed description can be found, e.g. in (Henderson & Lewis, 1998; Bamler & Hartl, 1998). After the SAR processing of the two

scenes individually, they are co-registered with sub-pixel accuracy. A spectral filtering reduces the slight decorrelation due to the different incidence angles and improves the signal-to-noise ratio. Then the actual interferogram generation follows calculating the conjugate complex product of the two complex datasets. After the reduction of the phase ramp corresponding to the flat Earth, the interferogram shows the phase differences similar to contour lines. The absolute phase is estimated from the relative phase during the phase unwrapping step and finally converted into terrain height. The resulting DEM is geocoded.

The side-looking illumination and signal reception causes specific geometric characteristics in SAR images. In mountainous areas, the effects of radar shadow and layover affect the resulting DEM. Shadows are caused by slopes less than the so-called radar grazing angle (back-side of mountains, buildings), which is the incidence angle of the radar reduced by 90°. There, the terrain is not illuminated and no signal is returned. Shadow always affects the slope and the following area (Eineder & Holzner, 2000). On the other hand, layover is caused by slopes steeper than the radar incidence angle (front-side of mountains, buildings). Due to the high slope, the space-time relationship is inverted and the slope overlays the area in front of the slope. Layover affects areas before and after the slope (Henderson & Lewis, 1998).

SAR interferometry can be distinguished into one-pass and two-pass or multi-pass acquisition. For one-pass interferometry, two antennas are mounted on the same carrier, mostly airplanes. One of the antennas is sending the signal and receiving the backscatter, the second antenna is only receiving. During February 11–22, 2000, the Shuttle Radar Topography Mission (SRTM) imaged the Earth with the first space-borne single-pass SAR interferometer (Adam et al., 1999). For the second method, a single antenna is flown which sends and receives the signal during each overflight. The European Remote Sensing Satellites ERS-1/2 flown since 1991 are the most prominent examples. Besides the combination of two passes of one satellite, data acquisitions of two passes of both ERS satellites are used for InSAR in the so-called tandem mode.

The long mission duration of the ERS satellites is a big advantage compared to the only 11-day mission of SRTM. On the other hand, with ERS tandem data, DEM generation is currently limited to moderate terrain. As described above, layover and shadow affect the visibility and resolution of SAR sensors in hilly and mountainous terrain. Therefore, phase unwrapping of such data is difficult. The incidence angle of SRTM of 54° (ERS 23°) avoids layover in mountainous areas, restricting these problems to extremely steep areas. Additionally, the single-pass observation avoids temporal decorrelation and artefacts through atmospheric delay (Eineder et al., 2000). The resulting SRTM DSM is of high quality due to its viewing geometry and high coherence (Eineder & Holzner, 2000).

3. DSM INTEGRATION

The common method up to now is the DSM generation from scratch, i.e. a completely new DSM is generated from a new data set. On the other hand, worldwide coverage with DEM is already available. For example, since 1996 GTOPO30 is accessible, a global digital elevation model with a horizontal grid spacing of 30 arc seconds (approximately 1 km). Data of the SRTM mission in 2000 refined the globally available DEM (80% of Earth's land mass) to a resolution of 3 arc seconds and much better height accuracy.

When different DEM exist, they are often combined by DEM fusion. The observed scene is unique, so it seems natural to obtain only a single DEM instead of having several individual DEM. Thereby, the density of reliable information increases resulting in more precise DEM than with individual DEM. The availability of several measures of the elevation for a given point also increases the accuracy of the fused DEM with respect to the individual DEM (Tannous & Le Goff, 1996, Reinartz et al., 2005). Another approach presented in this paper is the combination of different data sources during DSM generation. This data integration covers also the described advantages of data fusion. It is suggested when a single data set is prior to the other ones, e.g. a new data acquisition compared to much older DEM. Especially in cases with existing DEM having lower resolutions as the new data set, the integration of single points in 'holes' instead of a complete fusion seems more suitable.

The most promising approach to integrate single information is the input of points from the existing InSAR DSM into large areas without points in the new data set. Such areas can be found after the triangulation. When the size of a triangle is above a threshold, additional points are integrated that are located inside this triangle.

The selection of the threshold depends on the data set itself. It should be determined in dependence on the resolution of the existing DSM, the resolution of the DSM to be generated, as well as on the density of the given point cloud. The selection process for the test data set is discussed in Chapter 4. The implemented program needs as input the threshold in number of pixels. A threshold in square meters would also be meaningful since the triangulation result is independent of final resolution. However, since points have to be integrated only into triangles comprising pixels without points, a limiting pixel number is chosen.

3.1 Iterative Point Integration

The 3D points, which are the conjugate points received by the matching process transformed into the object space, are connected by a TIN during triangulation. For each resulting triangle, the enclosed area can be calculated.

Areas with a low point density result in DSM with low reliability. To prevent such areas, which are denoted by large triangles after Delauney triangulation, additional information is integrated from an existing DSM. A single additional point changes not only the shape of the triangle, where it is put inside, but also the surrounding triangles (Figure 2).
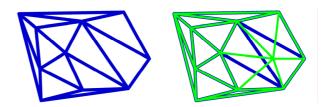

Figure 2. Changes in TIN by integrating a single point.

Therefore, in the first realization of the point integration, a single point is added to the triangle with the largest area. Then the areas of all triangles of the new TIN are calculated resulting in a new largest triangle. This point adding is continued until the area of the largest triangle is below the defined threshold.

Figure 3 shows the resulting point distribution for a part of the test area in southern Bavaria. The different point density of the original point cloud (shown in green) can be easily seen. Integrated points from the existing DSM marked in red are evenly distributed in large 'holes'.
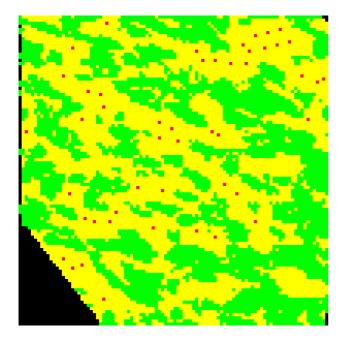
Figure 3. Resulting distribution by iterative point integration. Green = Pixel with SPOT 3D point. Red = Pixel with integrated point ($n_i = 48$). Yellow = Pixel to interpolate. Threshold = 20 pixels.

Ratio r of triangle area vs. threshold	Number of new points	Number of lines l	Distribution of new points
$1 \leq r < 2$	1	1	
$2 \leq r < 3$	3	2	
$3 \leq r < 6$	6	3	
$6 \leq r < 10$	10	4	
In general: $\displaystyle\sum_{i=1}^{l-1} i \leq r < \sum_{i=1}^{l} i$	$\displaystyle\sum_{i=1}^{l} i$	l	…

Table 1: Distribution and number of new points for integration into triangles larger than the threshold.

The described iterative algorithm delivers reliable results but is very slow. For each new point the complete TIN has to be checked for the largest triangle to define the new point and which triangles are changed by it. For large data sets (the test area contains 6 Mio. triangles, up to 100 000 points are integrated) this needs some time even on fast computers. Therefore, the algorithm was developed further to integrate multiple points at once.

3.2 Multiple Point Integration

The described point integration algorithm is made faster by integrating not only single points but multiple points in very

large triangles (area > 2 · threshold). Simultaneously points are integrated into all triangles larger than the threshold. After the integration only one new triangulation is necessary.

The number of points added to a triangle is defined by the ratio of triangle area vs. threshold. The number is slightly increased to fill a complete new line of new points (compare Table 1). The new points are integrated using a coordinate system defined by two sides and one vertex of each triangle. The two other vertices correspond to "1" on the coordinate axis. The points are then located at positions with distances $1/(l+2)$ on both axes forming lines (l = number of lines).

The result is shown in Figure 4 for the same part of the test area as shown in Figure 3. The number of points added ($n_m = 45$) is similar to the number integrated iteratively ($n_i = 48$). The distribution of the new points is comparable to the iteratively inserted points too. Exceptions occur only when triangles slightly below the threshold are changed due to a new point nearby (compare upper right corner in Figure 4). This can be eluded by choosing a slightly lower threshold. Therefore, the much faster multiple point integration can be taken instead of the time consuming iterative point integration.
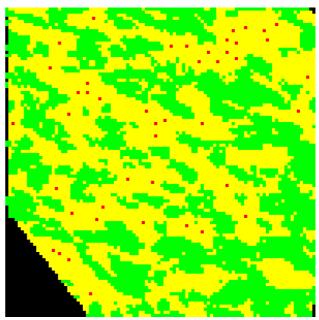

Figure 4. Resulting distribution by multiple point integration. Colours as in Figure 3. Threshold = 20 pixel. Number of integrated points $n_m = 45$.

4. COMPARISONS AND DISCUSSION

The test area chosen for this study is a region of about 40 km × 50 km in south-eastern Bavaria. Elevations range from 400 to 2000 m in a mostly hilly, post-glacial landscape including lakes and also mountains of the German Alps (Figure 1). It allows the comparison of DSM for different land surface shapes, including forest and steep terrain. Here also much knowledge exists from previous studies (e.g. Reinartz et al., 2004).

The SPOT HRS data have been acquired on October 1, 2002 with a sun elevation of 38° and nearly no clouds. The DSM is generated as described in Chapter 2 with a resolution of 25 m. The ground reference data comprises four regions with a grid spacing of 5 m and an overall size of about 5 × 5 km². They are derived by laser scanning representing the Earth surface

(DEM). The height accuracy is better than 0.5 m. For comparison purposes, they are averaged to a grid spacing of 25 m. Furthermore, different InSAR generated DSM were available. They have a spatial resolution of 25 m and a height accuracy of about 5 to 10 m (Jacobsen, 2004).

Before the integration of different DSM as well as before a DEM fusion, it has to be checked, if the overall height is comparable or if a possible bias between the differently generated DSM has to be taken into account. Therefore, the heights of the SPOT 3D points are compared to heights at the same positions in the available height models. Results are given in Table 2. The different data sets agree very well to the SPOT points with difference mean values of 1 m and below. The standard deviation is up to 10 m due to the wide elevation range of the test area. It is slightly smaller for the laser DEM since the four areas have a smaller elevation range. Due to the small values, no bias has been taken into account.

Input DSM	Resolution	Mean of difference	Std.dev. of difference
ERS	25 m	0.47 m	9.77 m
SRTM-C	25 m	1.06 m	6.11 m
SRTM-X	25 m	1.14 m	8.48 m
Laser	25 m	0.77 m	6.14 m
Laser	5 m	0.29 m	5.88 m

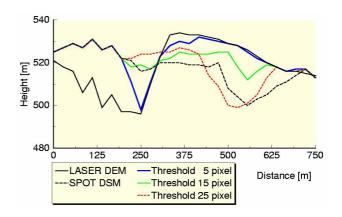Table 2: Comparison of SPOT 3D points to different existing DSM to determine a possible bias.

As described before, the area threshold depends on the analysed data set as well as the resolutions of the existing DSM and the DSM to be generated. It has to be defined for every data set individually. A too low value fills areas without points in the new data completely with existing information. A higher value reduces the input from the existing model. An analysis for the given SPOT data set is presented in Table 3. It shows that the data set is relatively dense since only a small number of points are integrated. With increasing threshold the number of triangles larger than the limit decreases proportional. The number of points inserted decreases non-proportional – in the analysed case from about double for a threshold of 5 pixels to just slightly higher for a threshold of 25 pixels (Table 3).
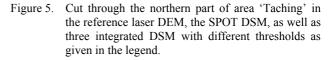
Threshold		Number of triangles		Points
Pixels	[m²]	Smaller	Larger	added
25	625	29154	160	188
15	375	28970	344	406
5	125	28018	1296	2412

Table 3: Execution of multiple point integration into 29314 triangles with different thresholds (resolution 25 m).

The effects of different thresholds can be best seen looking at profiles of the various height models along a given line (Figure 5). For comparison purposes, the reference laser DEM was used for point integration into the SPOT HRS data set. Additionally to the integrated DSM with three different thresholds, the reference DEM as well as the SPOT HRS DSM generated without point integration are given. The agreement in the first part results from a dense cloud of SPOT 3D points in this area. The laser DEM shows the landscape of a valley and a hill, which are covered by forest (information from topographic map), followed by another valley of open land (forest ends at

about 600 m). Between about 200 and 750 m are no points in the SPOT data set; the SPOT DSM is generated by interpolation. The integrated DSM show different adjustment steps to the laser DEM depending on the chosen threshold. The lower the chosen threshold is, the more points are integrated, and the higher is the agreement between resulting DSM and given reference DEM. For the further studies, a threshold of 20 Pixels (500 m²) is chosen.

Figure 5. Cut through the northern part of area 'Taching' in the reference laser DEM, the SPOT DSM, as well as three integrated DSM with different thresholds as given in the legend.

Finally, the resulting DSM are compared to the reference DEM. Since the DEM shows the Earth's surface, while the DSM is a surface model, a distinct difference is expected e.g. in forest areas. The comparison can be performed in several ways. One possibility is to evaluate only the points found during the matching and therefore are highly accurate homologous points. Results are shown at the beginning of this chapter while investigating a possible bias. In the integrated DSM, a further class of integrated points can be compared showing of course a high agreement when compared to the same DSM that was used for the point integration. The comparison to a different DSM shows only deviations between these two models and gives no result for the new integrated DSM.

Next an area oriented analysis has been carried out. For this approach, it should be distinguished between at least two types of classes – forest and non-forest areas – due to the described discrepancy of the DSM and the reference DEM. Results for the interpolated SPOT HRS data set as well as three integrated DSM are presented in Table 4. The statistic values agree very

DSM	Forest area		Non-forest area	
	Mean height diff. [m]	Std. Dev. [m]	Mean height diff. [m]	Std. Dev. [m]
SPOT	7.99	9.16	-0.54	5.26
SPOT + SRTM-C	9.94	9.63	-0.62	4.81
SPOT + SRTM-X	8.74	8.95	-0.59	5.03
SPOT + ERS	6.98	8.54	-0.57	4.75

Table 4: Comparison of integrated and non-integrated SPOT HRS DSM to the reference DEM for selected areas differentiated by surface types.

well for all DSM. Mean height differences are in the order of the analysis of the single points (Table 2); whereas the standard deviation is slightly reduced. This follows from the distribution of SPOT HRS points mainly in non-forest areas (about 80%). In forest areas, all values are of same order too. Here, more information originates from the integrated DSM since only 10% of the pixels contain a SPOT 3D point (32% of pixels in non-forest area). The meaning of the mean height differences in forest areas is discussed in detail in (Reinartz et al., 2005).

Another good possibility to analyse the consistency of different DSM is the evaluation of profiles along a given line. Results of such a comparison have been already discussed in context with Figure 5 and show for other examples that the integration of points leads to results closer to the real world If a sufficient accurately DSM is used.

5. CONCLUSIONS AND OUTLOOK

From different data sets of SPOT stereo image pairs and InSAR elevation models, a DSM was generated using the new approach of point integration. With multiple point integration, a large number of points are inserted into areas with less dense information at the same time. It is much faster and delivers similar results compared to single point integration. The threshold for the selection of areas to integrate points has to be chosen in dependence of the actual data sets.

The received absolute accuracy of terrain heights is in the order of 1 to 2 m (mean height error), with standard deviations of about 6 m for single points and 7 to 8 m for the interpolated SPOT DSM without integration of additional points in comparison to the reference DEM. After the integration of different InSAR DSM, the mean height error is in the same order, but with slightly reduced standard deviations (6 to 7 m). Differentiating into different land use classes gives similar mean height errors with a reduced standard deviation in non-forest areas and larger height differences in forest areas.

In future work the results of the DEM integration will be compared to results of DEM fusion approaches. The influence of different area thresholds will be analysed during the integration of InSAR DSM information into the SPOT 3D point dataset also for differently steep terrain.

REFERENCES

Ackermann, F., 1984. High precision digital image correlation. In: *Proceedings of the 39th Photogrammetric Week 1983*, Stuttgart University, Germany, Vol. 9 of the reports of the Institute of Photogrammetry.

Adam, N., Eineder, M., Breit, H., Suchandt, S., 1999. Shuttle Radar Topography Mission (SRTM): DLR's interferometric SAR processor for the generation of a global digital elevation model. In: *Proceedings of the Workshop on ERS SAR Interferometry FRINGE'99*, Liège, Belgium.

Baltsavias, E.P., 1999. A comparison between photogrammetry and laser scanning. *ISPRS Journal of Photogrammetry & Remote Sensing*, 54, pp. 83–94.

Bamler, R., Hartl, P., 1998. Synthetic aperture radar interferometry (Topical Review). In: *Inverse Problems*, No. 14, pp. R1–R54.

Bourke, P., 1989. Triangulate – Efficient triangulation algorithm suitable for terrain modelling. http://astronomy.swin.edu.au/~pbourke/terrain/triangulate/ (accessed 21 March 2005).

Eineder, M., Bamler, R., Adam, N., Suchandt, S., Breit, H., Steinbrecher, U., Rabus, B., Knöpfle, W., 2000. Analysis of SRTM interferometric X-band data: First results. In: *Proceedings of the IGARSS 2000*, Honolulu, Hawaii, Vol. VI, pp. 2593–2595.

Eineder, M., Holzner, J., 2000. Interferometric DEMs in alpine terrain – Limits and options for ERS and SRTM. In: *Proceedings of the IGARSS 2000*, Honolulu, Hawaii, Vol. VII, pp. 3210–3212.

Förstner, W., Gülch, E., 1987. A fast operator for detection and precise location of distinct points, corners and centers of circular features. In: *ISPRS Intercommission Workshop*, Interlaken, Switzerland.

Guoan, T., 2000. *A Research on the Accuracy of Digital Elevation Models*. Science Press, Beijing, New York.

Heipke, C., Kornus, W., Pfannenstein, A., 1996. The evaluation of MEOSS airborne 3-line scanner imagery – processing chain and results. *Photogrammetric Engineering and Remote Sensing*, 62(3), pp. 293–299.

Henderson, F.M., Lewis, A.J., (Ed.s), 1998. *Manual of Remote Sensing, Vol. 2: Principles and Applications of Imaging Radar.* John Wiley & Sons, Inc., New York, Chichester, Weinheim, 3rd edition.

Jacobsen, K., 2004. DEM generation from satellite data. In: Goossens, R. (Ed.): *Remote Sensing in Transition, Proceedings of the 23rd EARSeL Symposium 2003*, Ghent, Belgium, pp. 513–525.

Lehner, M., Gill, R.S., 1992. Semi-automatic derivation of digital elevation models from stereoscopic 3-line scanner data. In: *International Archives of Photogrammetry and Remote Sensing*, Washington, USA, Vol. XXIX, Part B4, pp. 68-75.

Reinartz, P., Lehner, M., Müller, R., Schroeder, M., 2004. Accuracy analysis for DEM and orthoimages derived from SPOT HRS stereo data without using GCP. In: *XXth ISPRS Congress*, Istanbul, Turkey.

Reinartz, P., Lehner, M., Hoja, D., Müller, R., Schroeder, M., 2005. Comparison and fusion of DEM derived from SPOT-5 HRS and SRTM data and estimation of forest heights. In: *Global Development in Environmental Earth Observation from Space, Proceedings of the 25th EARSeL Symposium*, Porto, Portugal.

Tannous, I., Le Goff, F., 1996. An integrated methodology for DEM computation through the fusion of interferometric, radargrammetric and Photogrammetric data. In: *Proceedings of the ERS SAR Interferometry Workshop FRINGE 1996*, Zurich, Switzerland.